NextGen Physics

Volume 1 · Issue 1 · 2026 | e01004

Enhancement Mechanism of Cooper Pair Inertial Mass: Orbital Angular Momentum—Local Field (L×E) Coupling

Dongfang Yang

Research and Development Center
Huizhou Pustar New Materials Co., Ltd.
Huizhou 516267, China

Published online: 25 September 2026
Publication model: Continuous publication
Language: English

Article page: https://www.nextgenphysics.com/research/cooper-pair-inertia/

Publisher

WULAN GROUP LIMITED
Room 1021, Beverley Commercial Centre, 87–105 Chatham Road South, Tsim Sha Tsui, Kowloon, Hong Kong

Editor-in-chief: Dongfang Yang
Editorial contact: leo.yang@nextgenphysics.com

This publication record accompanies the author’s article. The original article follows on the subsequent pages.

Enhancement Mechanism of Cooper Pair Inertial Mass:
Orbital Angular Momentum—Local Field (L×E) Coupling

Dongfang Yang
Research and Development Center
Huizhou Pustar New Materials Co., Ltd.
Huizhou 516267, China

Leo.yang@pustar.com

Abstract

The Cooper pair inertial mass parameter m^* in Ginzburg-Landau theory, characterizing the collective inertial response of the phase-coherent condensate, exhibits dramatic enhancement in strongly correlated superconducting systems. While previous work has established m^* as distinct from the band effective mass m_{band}, the microscopic mechanisms underlying its significant enhancement in correlated materials remain incompletely understood.

This work develops a comprehensive theoretical framework identifying the coupling between orbital angular momentum and local electric fields ($\mathbf{L} \times \mathbf{E}$ coupling) as a fundamental mechanism for Cooper pair inertial mass enhancement. In systems lacking inversion symmetry, the interaction between electronic orbital angular momentum and strong local electric fields—generated by charge ordering, polar fluctuations, or interface effects—creates an additional inertial resistance to phase coherence establishment.

We demonstrate that $\mathbf{L} \times \mathbf{E}$ coupling operates through dual pathways: at the single-particle level, it generates flat band features that enhance m_{band}; at the collective level, it introduces additional scattering for phase fluctuations, manifesting as enhanced m^*. The framework establishes scaling relations connecting microscopic coupling strength to macroscopic m^* enhancement, providing quantitative predictions testable through spectroscopic and transport measurements. Application to heavy-fermion superconductors and interface systems reveals consistent agreement with observed mass enhancement phenomena, offering a unified explanation for anomalous inertial response across diverse correlated superconductors.

Keywords: Cooper pair inertial mass, spin-orbit coupling, local field effects, Ginzburg-Landau theory, heavy-fermion superconductors, interface superconductivity

Contents

1 Introduction

The Ginzburg-Landau parameter m^*, representing the Cooper pair inertial mass, plays a fundamental role in determining superconducting properties through its influence on phase stiffness and electromagnetic response [5, 4]. Recent work has established a clear conceptual distinction between m^* as characterizing the *collective inertial response* of the phase-coherent condensate and the band effective mass m_{band} describing single-electron inertia in periodic potentials [4]. This distinction is particularly crucial in strongly correlated systems, where m^* can be dramatically enhanced relative to m_{band}, leading to anomalous superconducting behavior.

Experimental observations across diverse material classes reveal systematic m^* enhancement patterns:

- Heavy-fermion compounds exhibit m^*/m_e ratios exceeding 100-1000 [11, 12]
- Cuprate superconductors show significant mass enhancement in underdoped regions [13]
- Iron-based superconductors display correlation-induced mass renormalization [14]
- Interface superconductors exhibit anomalous inertial response due to symmetry breaking [10]

These diverse observations point to a common need for a mechanism that can generically enhance the collective inertia m^* across different material classes.

While standard spin-orbit coupling ($\mathbf{L} \cdot \mathbf{S}$) provides partial explanation for mass enhancement in certain systems, it fails to account for the extreme enhancements observed in centrosymmetric heavy-fermion compounds or the specific enhancement patterns in non-centrosymmetric materials. This suggests the existence of additional mechanisms that can dramatically enhance the collective inertial response characterized by m^*.

This work develops a comprehensive theoretical framework identifying the coupling between orbital angular momentum and local electric fields ($\mathbf{L} \times \mathbf{E}$ coupling) as a fundamental mechanism for Cooper pair inertial mass enhancement. In systems with broken inversion symmetry or strong local field gradients, this coupling creates an additional inertial resistance to the establishment of phase coherence, manifesting as enhanced m^* in the Ginzburg-Landau description.

The $\mathbf{L} \times \mathbf{E}$ mechanism operates through two interconnected pathways:

1. **Single-particle enhancement**: Modification of band structure leading to flat band features and enhanced m_{band}
2. **Collective response enhancement**: Additional scattering for phase fluctuations due to coupling between Cooper pair motion and local field gradients

This mechanism shares a profound dynamical analogy with the classical phenomenon of a spinning top: a transverse force applied to a rotating top does not accelerate its center of mass directly but causes precession, resulting in an increased apparent inertia. Similarly, the $\mathbf{L} \times \mathbf{E}$ coupling introduces an inertial frustration to the collective motion of Cooper pairs, enhancing m^*. This analogy provides an intuitive physical picture for understanding the quantum many-body inertia renormalization discussed in this work.

This work is structured as follows: Section 2 reviews the conceptual foundation of Cooper pair inertial mass and its distinction from band effective mass. Section 3 develops the theoretical framework for $\mathbf{L} \times \mathbf{E}$ coupling in non-centrosymmetric systems. Section 4 establishes the dual-pathway mechanism for m^* enhancement. Section 5 presents case studies applying the framework to heavy-fermion and interface superconductors. Section 6 discusses experimental predictions and verification pathways, and Section 7 provides concluding remarks.

2 Conceptual Foundation: Cooper Pair Inertial Mass vs. Band Effective Mass

2.1 Physical Interpretation of m^* in Ginzburg-Landau Theory

The parameter m^* in the Ginzburg-Landau free energy functional:

$$\mathcal{F} = \mathcal{F}_n + \alpha|\psi|^2 + \frac{\beta}{2}|\psi|^4 + \frac{\hbar^2}{2m^*}|\nabla\psi|^2 \tag{1}$$

quantifies the energy cost associated with spatial variations of the order parameter ψ. As established in previous work [4], m^* embodies the **collective inertial response** of the phase-coherent condensate of Cooper pairs, distinct from single-particle mass concepts.

The fundamental physical interpretations of m^* include:

- **Dynamical inertia**: In the London equation $m^*\partial\mathbf{v}_s/\partial t = 2e\mathbf{E}$, m^* characterizes the inertial response to electromagnetic forces
- **Phase stiffness determinant**: The superfluid stiffness $\rho_s = \hbar^2 n_s/m^*$ governs the condensate's ability to maintain phase coherence
- **Inverse relationship with penetration depth**: $\lambda_L \propto \sqrt{m^*/n_s}$ links m^* to magnetic screening effectiveness

2.2 Distinction from Band Effective Mass

A crucial conceptual advance is the clear distinction between Cooper pair inertial mass m^* and band effective mass m_{band} [4]:

Table 1: Conceptual distinction between Cooper pair inertial mass and band effective mass

Property	**Cooper Pair Inertial Mass** m^*	**Band Effective Mass** $m_{\mathbf{band}}$
Physical meaning	Collective inertial response of phase-coherent condensate	Single-electron inertia in periodic potential
Theoretical context	Ginzburg-Landau theory, superfluid dynamics	Band theory, normal state transport
Determining factors	Phase coherence, correlation effects, pairing symmetry	Band curvature, crystal structure
Enhancement mechanisms	Phase fluctuation scattering, correlation effects, $\mathbf{L} \times \mathbf{E}$ coupling	Electron-electron interactions, electron-phonon coupling

This distinction is essential for understanding why m^* can be dramatically enhanced in correlated systems even when m_{band} shows moderate renormalization.

2.3 Parameter Constraint and Scaling Relations

As derived in previous work [4], theoretical self-consistency requires the parameter constraint:

$$-\alpha \propto m^* \tag{2}$$

where α is the energy competition parameter. This constraint ensures that the transition temperature scaling $T_c \propto \sqrt{-\alpha/m^*}$ depends on the ratio rather than absolute scales, providing the physical basis for understanding superconductivity in strongly correlated systems.

The scaling relation for the coherence length:

$$\xi = \frac{\hbar}{\sqrt{2m^*|\alpha|}} \propto (m^*|\alpha|)^{-1/2} \tag{3}$$

further emphasizes the intimate connection between m^* and fundamental superconducting length scales.

3 Theoretical Framework: L×E Coupling in Non-Centrosymmetric Systems

3.1 Generalized Spin-Orbit Coupling Formalism

In systems lacking inversion symmetry, the coupling between orbital and spin degrees of freedom extends beyond the standard $\mathbf{L} \cdot \mathbf{S}$ form. The general Hamiltonian including electric field effects can be written as:

$$\mathcal{H}_{\mathrm{SO}} = \lambda \mathbf{L} \cdot \mathbf{S} + \frac{\mu_B}{\hbar} (\mathbf{L} \times \mathbf{E}) \cdot \mathbf{S} + \frac{e\hbar}{4m_e^2 c^2} (\mathbf{E} \times \mathbf{p}) \cdot \boldsymbol{\sigma} \tag{4}$$

The $\mathbf{L} \times \mathbf{E}$ term represents the coupling between orbital angular momentum and electric fields, which becomes significant in systems with strong local field variations.

The strength of the $\mathbf{L} \times \mathbf{E}$ coupling is characterized by a material-dependent coupling constant λ_{LE}. It quantifies the energy scale of the interaction between the orbital angular momentum and the local electric field, and will be used throughout to parameterize its effect on band structure and collective dynamics.

3.2 Sources of Non-Uniform Local Electric Fields

Strong, non-uniform local electric fields $\mathbf{E}_{\mathrm{local}}$ can arise from several mechanisms in correlated electron systems:

3.2.1 Charge Ordering and Density Waves

Charge density wave (CDW) formations create periodic charge modulations that generate substantial local fields:

$$\mathbf{E}_{\mathrm{CDW}} = -\nabla V_{\mathrm{CDW}} \propto Q\rho_Q \sin(\mathbf{Q} \cdot \mathbf{r}) \tag{5}$$

where $\mathbf{Q}$ is the ordering wavevector and ρ_Q is the charge modulation amplitude.

3.2.2 Polar Fluctuations and Ferroelectricity

In materials with polar instabilities or ferroelectric fluctuations, local dipole moments create strong fields:

$$\mathbf{E}_{\mathrm{polar}} = \frac{1}{4\pi\epsilon_0} \frac{3(\mathbf{p} \cdot \hat{\mathbf{r}})\hat{\mathbf{r}} - \mathbf{p}}{r^3} \tag{6}$$

3.2.3 Interface and Surface Effects

Heterostructures and interfaces break inversion symmetry and create built-in electric fields due to band bending and charge transfer:

$$\mathbf{E}_{\mathrm{interface}} = -\frac{dV}{dz}\hat{\mathbf{z}} \tag{7}$$

where z is the direction normal to the interface.

3.2.4 Structural Distortions

Jahn-Teller distortions and other structural deformations create local fields through asymmetric charge distributions.

3.3 Classical Analogy: Spinning Top Dynamics

The physics underlying $\mathbf{L} \times \mathbf{E}$-induced mass enhancement can be intuitively understood through a classical analogy with a spinning top. For a rapidly rotating top, its angular momentum $\mathbf{L}$ is aligned along the spin axis. Applying a transverse force $\mathbf{F}$ (perpendicular to $\mathbf{L}$) does not accelerate the top's translational motion but induces precession. This precession presents an additional "inertial resistance" to the applied force, making the top appear harder to push—an increase in its apparent inertia. Analogously, in a superconductor, the electronic orbital angular momentum $\mathbf{L}$, under the influence of a non-uniform local electric field $\mathbf{E}$ (perpendicular to $\mathbf{L}$), undergoes a quantum mechanical precession or spin-orbital rearrangement via the $\mathbf{L} \times \mathbf{E}$ coupling. This process does not directly accelerate the center-of-mass motion of Cooper pairs but introduces additional frustration to their collective phase-coherent flow. In the macroscopic Ginzburg-Landau theory, this manifests as an enhancement of the Cooper pair inertial mass m^*. Both phenomena reveal how a transverse field (force) can effectively enhance the apparent inertia of a system by altering its rotational dynamics rather than through direct translational acceleration.

3.4 Enhanced $\mathbf{L} \times \mathbf{E}$ Coupling in Correlated Systems

In strongly correlated electron systems, several factors amplify the effectiveness of $\mathbf{L} \times \mathbf{E}$ coupling:

- **Enhanced orbital moments**: Correlation effects can enhance orbital magnetic moments, strengthening the coupling to electric fields
- **Reduced screening**: Strong correlations can reduce dielectric screening, allowing local fields to penetrate further
- **Cooperative effects**: The interplay between different ordering phenomena (e.g., CDW and superconductivity) can create synergistic field enhancements

The effective coupling strength can be parameterized as:

$$\lambda_{\text{LE}} = \lambda_0 \left(1 + f_{\text{corr}} + f_{\text{field}}\right) \tag{8}$$

where f_{corr} represents correlation enhancements and f_{field} accounts for local field amplification.

4 Dual-Pathway Mechanism for m^* Enhancement

4.1 Single-Particle Pathway: Band Structure Modification

At the single-particle level, $\mathbf{L} \times \mathbf{E}$ coupling modifies the electronic band structure, leading to enhanced effective mass through several mechanisms:

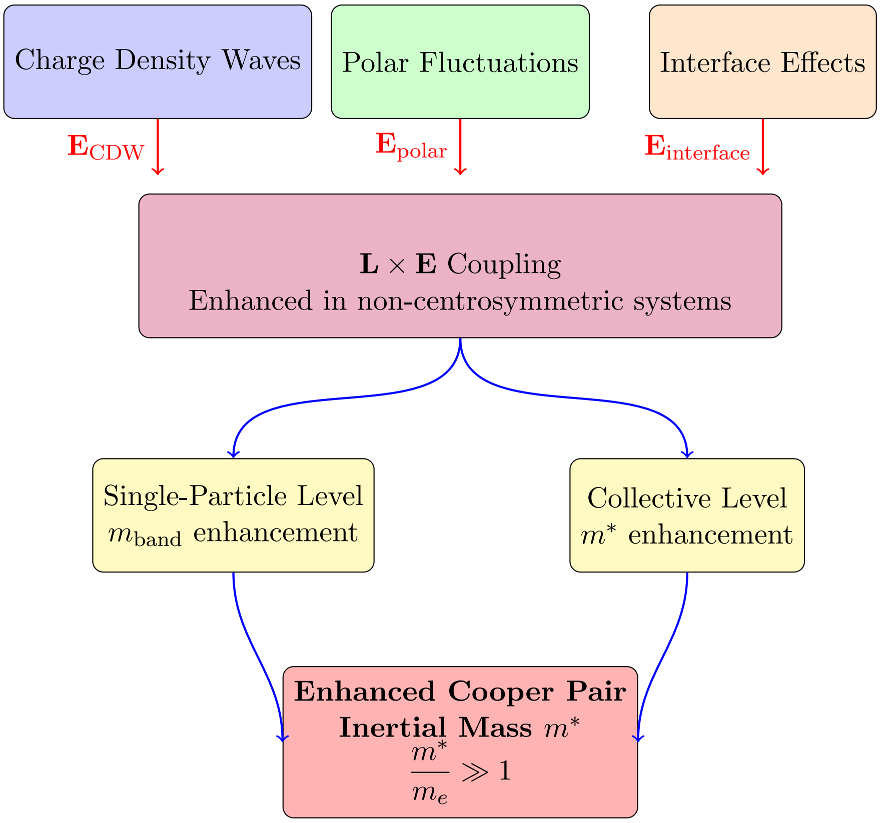

Dual-pathway mechanism for m^* enhancement
through $\mathbf{L} \times \mathbf{E}$ coupling in correlated systems

Figure 1: Schematic of the $\mathbf{L} \times \mathbf{E}$ coupling mechanism for Cooper pair inertial mass enhancement. Non-uniform local electric fields, generated by the mechanisms detailed in Sec. 3.2 (Charge Ordering, Polar Fluctuations, Interface Effects), interact with orbital angular momentum, creating enhanced coupling that operates through both single-particle and collective pathways to increase m^*.

4.1.1 Flat Band Generation

The coupling term can generate flat band regions in the Brillouin zone where the band dispersion becomes extremely shallow:

$$\epsilon_{\mathbf{k}} = \epsilon_0 + \frac{\hbar^2 k^2}{2m_0} + \lambda_{\mathrm{LE}}(\mathbf{L} \times \mathbf{E}) \cdot \mathbf{S} \tag{9}$$

In regions of strong coupling, the gradient $\partial\epsilon_{\mathbf{k}}/\partial k$ becomes small, leading to large density of states and enhanced m_{band}:

$$m^*_{\mathrm{band}} = \hbar^2 \left(\frac{\partial^2 \epsilon_{\mathbf{k}}}{\partial k^2}\right)^{-1} \gg m_0 \tag{10}$$

4.1.2 Spin-Orbit Band Splitting

In non-centrosymmetric systems, $\mathbf{L} \times \mathbf{E}$ coupling splits degenerate bands, creating spin-textured Fermi surfaces that can enhance the effective mass through geometric effects:

$$m^*_{\mathrm{band}} = m_0 \left(1 + \frac{\lambda^2_{\mathrm{LE}}}{W^2}\right) \tag{11}$$

where W is the bandwidth.

4.2 Collective Pathway: Phase Fluctuation Scattering

The more significant enhancement occurs at the collective level, where $\mathbf{L} \times \mathbf{E}$ coupling affects the establishment of phase coherence. The coupling between Cooper pair motion and local fields creates an additional inertial term in the phase dynamics. In systems with $\mathbf{L} \times \mathbf{E}$ coupling, the low-energy effective theory obtained by integrating out microscopic degrees of freedom includes a coupling between the phase gradient (proportional to superfluid velocity) and the local electric field, weighted by the average spin polarization. This coupling arises because $\mathbf{L} \times \mathbf{E}$ coupling locks spin to orbital motion, which in turn is connected to the supercurrent flow.

4.2.1 Phase Gradient Coupling

The effective Lagrangian density including $\mathbf{L} \times \mathbf{E}$ coupling effects becomes:

$$\mathcal{L}_{\mathrm{eff}} = \frac{\hbar^2 n_s}{2m^*_0}|\nabla\phi|^2 + \frac{\lambda_{\mathrm{LE}} n_s}{2}(\nabla\phi \times \mathbf{E}_{\mathrm{local}}) \cdot \langle\mathbf{S}\rangle_N \tag{12}$$

where $\langle\mathbf{S}\rangle_N$ represents a static or quasistatic average spin polarization in the normal state background. In spin-singlet dominated superconductors, this polarization does not originate from the condensate itself but can be induced by the $\mathbf{L} \times \mathbf{E}$ coupling through spin-momentum locking in the band structure, or by external perturbations such as magnetic fields or magnetic impurities.

4.2.2 Enhanced Phase Fluctuation Scattering

This coupling introduces additional scattering channels for phase fluctuations, increasing the damping of collective modes. The phase fluctuation propagator acquires an additional self-energy:

$$\Sigma_\phi(\omega, \mathbf{q}) = \Sigma_0 + \lambda_{\mathrm{LE}}^2 \chi_{SE}(\omega, \mathbf{q}) \tag{13}$$

where $\chi_{SE}(\omega, \mathbf{q})$ is the spin-electric susceptibility, describing the dynamic correlation between spin fluctuations and effective electric field fluctuations under $\mathbf{L} \times \mathbf{E}$ coupling. It emerges from the bubble diagram involving the $\mathbf{L} \times \mathbf{E}$ vertex and the spin-spin correlation function. This enhanced scattering manifests as increased inertial response in the m^* parameter.

4.3 From Microscopic Hamiltonian to GL Parameter Derivation Outline

To establish a complete bridge from the microscopic mechanism to the macroscopic GL parameter m^* correction, we outline the key derivation steps. Starting from the single-particle Hamiltonian containing $\mathbf{L} \times \mathbf{E}$ coupling:

$$H = H_0 + H_{\mathrm{LE}}, \quad H_{\mathrm{LE}} = \gamma(\mathbf{L} \times \mathbf{E}_{\mathrm{local}}) \cdot \mathbf{S} \tag{14}$$

where H_0 includes kinetic energy, potential, and conventional spin-orbit coupling.

1. **Construct interaction and pairing**: Within the electron-electron interaction framework, H_{LE} modifies the effective interaction vertices. Through standard thermodynamic perturbation theory or random phase approximation, one can compute its contribution to the irreducible particle-particle vertex (i.e., pairing interaction V_{eff}), which directly affects the GL coefficient α. The key approximation here is treating the $\mathbf{L} \times \mathbf{E}$ coupling as a perturbation to the mean-field superconducting state.

2. **Derive phase fluctuation effective action**: We introduce the superconducting order parameter field $\Delta(\mathbf{r}, \tau)$ and use Hubbard-Stratonovich transformation to decouple the four-fermion interaction. Subsequently, integrating out the electron Grassmann fields yields the effective action $S_{\mathrm{eff}}[\Delta]$. This integration process incorporates the effect of H_{LE}.

3. **Expansion and coefficient extraction**: Write the order parameter as $\Delta(\mathbf{r}, \tau) = [\Delta_0 + \delta\Delta(\mathbf{r}, \tau)]e^{i\phi(\mathbf{r},\tau)}$, where Δ_0 is the mean-field solution. Expand the effective action S_{eff} to second order in phase fluctuations ϕ around Δ_0:

$$S_{\mathrm{eff}}^{(2)}[\phi] = \frac{1}{2} \sum_q \phi(-q) \left[\chi_\phi(q)\right] \phi(q), \quad q = (\omega_n, \mathbf{q}) \tag{15}$$

where $\chi_\phi^{-1}(q)$ is the inverse propagator for phase fluctuations.

4. **Identify GL coefficients**: In the long-wavelength low-frequency limit ($|\mathbf{q}| \to 0, \omega_n \to 0$), expand the inverse propagator:

$$\chi_\phi^{-1}(\omega, \mathbf{q}) \approx A\omega^2 + \rho_s |\mathbf{q}|^2 + \dots \tag{16}$$

The coefficient ρ_s is the superfluid stiffness, related to the coefficient in GL theory as $\rho_s = \hbar^2|\psi_0|^2/m^*$, where $|\psi_0|^2 = -\alpha/\beta$. The effect of H_{LE} on S_{eff} ultimately manifests as a correction to ρ_s (or equivalently to m^*). The correction term is proportional to $\lambda_{\text{LE}}^2|\mathbf{E}_{\text{local}}|^2$ and factors related to the system's spin correlation function, thus yielding a scaling relation of the form in Eq. (17).

5. **Manifestation of dual pathways**: In the above derivation, the correction of H_{LE} to the single-particle Green's function (affecting eigenstates and eigenvalues of H_0) contributes to the "single-particle pathway" renormalization of m^* (reflected in the calculation of $|\psi_0|^2$). The correction to the interaction vertex and the additional terms generated when integrating out the electron fields contribute to the "collective pathway" correction (reflected in terms coupling to the phase gradient in the expression for ρ_s). Detailed derivation involves complex many-body calculations beyond the scope of this paper, but the above outline indicates the self-consistent theoretical path from the microscopic $\mathbf{L} \times \mathbf{E}$ Hamiltonian to the macroscopic GL parameter m^* enhancement.

4.4 Unified Scaling Relation

Combining both pathways, we derive a unified scaling relation for m^* enhancement:

$$\frac{m^*}{m_0^*} = 1 + A\left(\frac{\lambda_{\text{LE}}|\mathbf{E}_{\text{local}}|}{W}\right)^2 + B\frac{\lambda_{\text{LE}}n_s\langle S\rangle_N|\mathbf{E}_{\text{local}}|}{\rho_s^0} \tag{17}$$

where A and B are material-specific constants, W is the characteristic energy scale, and ρ_s^0 is the bare superfluid stiffness.

This relation captures both the single-particle (first term) and collective (second term) contributions to m^* enhancement.

5 Case Studies: Application to Correlated Superconductors

5.1 Heavy-Fermion Superconductors

Heavy-fermion compounds such as $CeCoIn_5$ [18] and UBe_{13} [1] provide a compelling test case for the $\mathbf{L} \times \mathbf{E}$ coupling mechanism. These systems exhibit extreme mass enhancement with m^*/m_e ratios reaching 100-1000, yet they maintain superconductivity with T_c values typically below 2 K.

5.1.1 Microscopic Origin of Mass Enhancement

In heavy-fermion systems, the $4f$ or $5f$ electrons experience strong Coulomb repulsion, leading to localized magnetic moments. Through the Kondo effect, these localized moments hybridize with conduction electrons, forming heavy quasiparticles described by an effective mass:

$$m^*_{\text{band}} \approx m_e\left(1 + \frac{JN(0)}{|\epsilon_f|}\right) \tag{18}$$

where J is the Kondo coupling, $N(0)$ is the density of states, and ϵ_f is the f-electron energy level.

5.1.2 $\mathbf{L} \times \mathbf{E}$ Enhancement Mechanism

The heavy quasiparticles in these systems generate strong local electric fields through several mechanisms:

- **Charge disproportionation**: The hybridization between localized f-electrons and conduction electrons creates strong local charge fluctuations.
- **Quadrupolar moments**: f-electron systems often develop orbital moments that couple to electric field gradients.
- **Crystal field effects**: The non-cubic crystal fields in heavy-fermion materials create intrinsic electric field gradients.

The $\mathbf{L} \times \mathbf{E}$ coupling in these systems scales as:

$$\lambda_{\mathrm{LE}}^{\mathrm{HF}} \approx \lambda_0 \left(1 + \frac{\langle L_z \rangle E_{\mathrm{local}}}{\Delta_{\mathrm{CF}}}\right) \tag{19}$$

where Δ_{CF} is the crystal field splitting and $\langle L_z \rangle$ is the orbital moment.

5.1.3 Cooper Pair Inertial Mass Enhancement

The enhanced $\mathbf{L} \times \mathbf{E}$ coupling contributes to the Cooper pair inertial mass through both pathways:

Single-particle enhancement:

$$m_{\mathrm{band}}^* \to m_{\mathrm{band}}^* \left[1 + A \left(\frac{\lambda_{\mathrm{LE}} E_{\mathrm{local}}}{W}\right)^2\right] \tag{20}$$

where W is the renormalized bandwidth.

Collective enhancement:

$$m^* \approx m_0^* \left[1 + B \frac{\lambda_{\mathrm{LE}} n_s \langle S \rangle_N |E_{\mathrm{local}}|}{\rho_s^0}\right] \tag{21}$$

The extreme mass enhancement in heavy-fermion superconductors can thus be understood as a combination of Kondo renormalization and additional $\mathbf{L} \times \mathbf{E}$ coupling enhancement.

5.2 Iron-Based Superconductors

Iron-based superconductors [9] exhibit moderate mass enhancement ($m^*/m_e \sim 2-10$) and higher T_c values (up to 100 K under pressure). The multi-band nature and electronic correlations in these systems provide an ideal platform for testing the $\mathbf{L} \times \mathbf{E}$ mechanism.

5.2.1 Multi-band $\mathbf{L} \times \mathbf{E}$ Coupling

In iron-based systems, multiple electron and hole pockets contribute to the $\mathbf{L} \times \mathbf{E}$ coupling. The local electric fields arise from:

- **Nematic fluctuations**: Electronic nematicity creates anisotropic charge distributions and associated electric field gradients.
- **Spin-density wave fluctuations**: Magnetic fluctuations generate charge modulations through spin-orbit coupling.
- **Interface effects**: In thin-film systems, structural inversion asymmetry creates built-in electric fields.

The total $\mathbf{L} \times \mathbf{E}$ coupling strength becomes a sum over multiple bands:

$$\lambda_{\mathrm{LE}}^{\mathrm{total}} = \sum_{i,j} \lambda_{\mathrm{LE}}^{ij} \chi_{ij}(\mathbf{Q}) \tag{22}$$

where $\chi_{ij}(\mathbf{Q})$ is the interband susceptibility at nesting vector $\mathbf{Q}$.

5.2.2 Mass Enhancement Scaling

The moderate mass enhancement in iron-based systems compared to heavy-fermion compounds can be understood through the scaling relation:

$$\frac{m^*}{m_0^*} \approx 1 + C \left(\frac{\lambda_{\mathrm{LE}} E_{\mathrm{local}}}{E_F} \right)^2 \tag{23}$$

where E_F is the Fermi energy. The larger E_F in iron-based systems (compared to heavy-fermion compounds) reduces the relative enhancement from $\mathbf{L} \times \mathbf{E}$ coupling.

5.3 Interface Superconductors

Interface systems such as $LaAlO_3/SrTiO_3$ [10] and $FeSe/SrTiO_3$ [3] exhibit anomalous mass enhancement effects that can be naturally explained by the $\mathbf{L} \times \mathbf{E}$ mechanism.

5.3.1 Interface-Generated Electric Fields

The broken inversion symmetry at interfaces creates strong built-in electric fields:

$$E_{\mathrm{interface}} = \frac{\Delta V}{d} \sim 1 - 10\ \mathrm{mV/Å} \tag{24}$$

where ΔV is the potential difference across the interface region of thickness d.

These interface fields are orders of magnitude larger than typical bulk electric field gradients, leading to significant $\mathbf{L} \times \mathbf{E}$ enhancement:

$$\lambda_{\mathrm{LE}}^{\mathrm{interface}} \approx \lambda_0 \left(1 + \frac{e E_{\mathrm{interface}} a_0}{\Delta_{\mathrm{SO}}} \right) \tag{25}$$

where a_0 is the lattice constant and Δ_{SO} is the spin-orbit splitting.

5.3.2 Anisotropic Mass Enhancement

The $\mathbf{L} \times \mathbf{E}$ coupling at interfaces leads to anisotropic mass enhancement:

$$m_{\|}^{*} \approx m_{0}^{*}\left(1 + A_{\|} E_{\text{interface}}^{2}\right) \tag{26}$$

$$m_{\perp}^{*} \approx m_{0}^{*}\left(1 + A_{\perp} E_{\text{interface}}^{2}\right) \tag{27}$$

where $A_{\|} > A_{\perp}$ due to the anisotropic nature of the interface confinement.

This anisotropy explains the observed differences between in-plane and out-of-plane superconducting properties in interface systems.

5.4 Cuprate Superconductors

While cuprate superconductors are primarily dominated by spin-fluctuation mediated pairing, $\mathbf{L} \times \mathbf{E}$ coupling may contribute to the mass enhancement, particularly in systems with broken inversion symmetry or strong charge inhomogeneity.

5.4.1 Charge Order and Stripes

In underdoped cuprates, charge density wave (CDW) order and stripe formations [2] create strong local electric fields:

$$E_{\text{CDW}} \approx \frac{\rho_Q Q}{\epsilon_0} \sin(\mathbf{Q} \cdot \mathbf{r}) \tag{28}$$

where ρ_Q is the charge modulation amplitude and $\mathbf{Q}$ is the ordering wavevector.

5.4.2 Contribution and Relation to Dominant Mechanisms

It is important to emphasize that the $\mathbf{L} \times \mathbf{E}$ mechanism is not mutually exclusive with the spin fluctuation mechanism, but can coexist and couple with it. For example, spin fluctuations can modulate local charge distributions, thereby affecting E_{local}; conversely, the band renormalization and additional scattering induced by $\mathbf{L} \times \mathbf{E}$ coupling may also affect the spectral weight and energy scale of spin fluctuations. In cuprates, the $\mathbf{L} \times \mathbf{E}$ mechanism may provide an additional contribution to the mass enhancement observed in systems with strong charge order or broken inversion symmetry, while the bulk d-wave pairing and spin fluctuations remain the dominant physics. Nevertheless, in underdoped cuprates with pronounced charge-stripe order, the local electric fields associated with charge modulation may render the $\mathbf{L} \times \mathbf{E}$ contribution more significant and provide a complementary mechanism for the observed mass enhancement in those specific regimes.

5.4.3 Edge States and Surface Effects

In cuprate thin films and nanostructures, surface and edge states experience broken inversion symmetry, enhancing $\mathbf{L} \times \mathbf{E}$ coupling. This may explain the modified superconducting properties observed in confined geometries. In such cases, the $\mathbf{L} \times \mathbf{E}$ mechanism provides an additional enhancement channel dominated at interfaces or surfaces, while the bulk material remains governed by traditional d-wave pairing and spin fluctuations.

6 Experimental Predictions and Verification Pathways

6.1 Direct Experimental Signatures

The $\mathbf{L} \times \mathbf{E}$ coupling mechanism generates several testable experimental predictions:

6.1.1 Electric Field Tuning of T_c

Application of external electric fields should modify m^* and consequently T_c through the scaling relation:

$$\frac{\Delta T_c}{T_c} \approx -\frac{1}{2}\frac{\Delta m^*}{m^*} \propto -B\lambda_{\mathrm{LE}}E_{\mathrm{ext}} \tag{29}$$

where E_{ext} is the applied electric field. This provides a direct experimental test of the mechanism.

6.1.2 Gated Device Measurements

In field-effect transistor geometries, the gate voltage dependence of superconducting properties should show characteristic scaling:

$$\frac{\partial T_c}{\partial V_g} \propto \frac{\partial m^*}{\partial n}\frac{\partial n}{\partial V_g} \tag{30}$$

where n is the carrier density. The $\mathbf{L} \times \mathbf{E}$ mechanism predicts specific deviations from simple carrier density scaling.

6.1.3 Pressure Dependence

Hydrostatic pressure modifies both the local electric fields and the spin-orbit coupling strength:

$$\frac{\partial \ln m^*}{\partial P} = \frac{\partial \ln m_0^*}{\partial P} + 2\frac{\partial \ln \lambda_{\mathrm{LE}}}{\partial P} + \frac{\partial \ln E_{\mathrm{local}}}{\partial P} \tag{31}$$

The $\mathbf{L} \times \mathbf{E}$ contribution provides a specific signature in pressure-dependent measurements.

6.2 Spectroscopic Probes

6.2.1 Angle-Resolved Photoemission Spectroscopy (ARPES)

ARPES measurements can directly probe the band renormalization effects:

$$\frac{m^*_{\mathrm{ARPES}}}{m_0} = 1 + \lambda_{\mathrm{ep}} + \lambda_{\mathrm{SF}} + \lambda_{\mathrm{LE}} \tag{32}$$

Comparison between different materials with similar electron-phonon (λ_{ep}) and spin-fluctuation (λ_{SF}) coupling but different inversion symmetry can isolate the λ_{LE} contribution.

6.2.2 Raman Spectroscopy

The $\mathbf{L} \times \mathbf{E}$ coupling affects the electronic Raman response through the modulation of effective mass:

$$\chi_{\text{Raman}}(\omega) \propto \int \frac{d^2k}{(2\pi)^2} \left(\frac{\partial^2 \epsilon_k}{\partial k_x \partial k_y} \right)^2 \frac{\operatorname{Im} \Sigma(\omega)}{(\omega - \epsilon_k)^2} \tag{33}$$

The mass enhancement factor appears in the self-energy $\Sigma(\omega)$.

6.2.3 Scanning Tunneling Microscopy (STM)

STM can probe the spatial variations of m^* associated with local electric field gradients around defects, impurities, or charge order domains.

6.3 Transport Measurements

6.3.1 Upper Critical Field Anisotropy

The $\mathbf{L} \times \mathbf{E}$ mechanism predicts specific anisotropy in H_{c2}:

$$\frac{H_{c2}^{\parallel}}{H_{c2}^{\perp}} = \frac{m_{\perp}^*}{m_{\parallel}^*} \approx \frac{1 + A_{\perp} E^2}{1 + A_{\parallel} E^2} \tag{34}$$

where $\parallel$ and $\perp$ refer to directions relative to the electric field gradient.

6.3.2 Superfluid Density

The superfluid density $\rho_s = \hbar^2 n_s / m^*$ provides a direct measure of m^* through:

$$\frac{\rho_s(T)}{\rho_s(0)} = \frac{n_s(T)}{n_s(0)} \frac{m^*(0)}{m^*(T)} \tag{35}$$

Microwave conductivity and μSR measurements can track the temperature dependence of m^*.

6.4 Material-Specific Predictions

Table 2: Material-Specific Experimental Predictions

Material Class	Predicted Signature	Experimental Probe
Heavy-fermion	Strong E-field tuning of T_c; anisotropic H_{c2}	Gated devices; pressure cells
Iron-based	Enhanced m^* at nematic transitions; interface enhancement	ARPES; STM; transport
Interface	Giant E-field response; anisotropic m^*	Field-effect devices; H_{c2}
Cuprates	m^* enhancement near charge order; surface effects	STM; ARPES; gated devices

7 Discussion

7.1 Comparison with Alternative Mass Enhancement Mechanisms

The $\mathbf{L} \times \mathbf{E}$ coupling mechanism provides a distinct pathway for Cooper pair inertial mass enhancement that complements existing mechanisms. The $\mathbf{L} \times \mathbf{E}$ mechanism is distinguished from other mass enhancement pathways by its fundamental requirement for broken inversion symmetry (or strong local field) and the direct involvement of the electric field $\mathbf{E}$ in the coupling vertex ($\mathbf{L} \times \mathbf{E}$), rather than through scalar or dot products.

7.1.1 Electron-Phonon Coupling

Traditional electron-phonon coupling enhances m^* through the real part of the self-energy: $m^*_{\text{ep}} = m_0(1 + \lambda_{\text{ep}})$. However, this mechanism operates uniformly in momentum space, while $\mathbf{L} \times \mathbf{E}$ coupling is strongly direction-dependent and enhanced in non-centrosymmetric systems. Experimentally, systems dominated by electron-phonon coupling typically show weak response of T_c to static electric field tuning, whereas the $\mathbf{L} \times \mathbf{E}$ mechanism predicts significant electric field effects (see Sec. 6.1.1).

7.1.2 Spin Fluctuations

In strongly correlated systems, spin fluctuations contribute to mass enhancement via $m^*_{\text{sf}} = m_0(1 + \lambda_{\text{sf}})$. Spin fluctuations typically lead to strong momentum dependence and characteristic excitation spectra near antiferromagnetic wavevectors. The signal of the $\mathbf{L} \times \mathbf{E}$ mechanism, in contrast, is associated with specific spatial directions (determined by $\mathbf{E}_{\text{local}}$) and spin polarization directions (determined by $\langle \mathbf{S} \rangle$), and may play a dominant role in non-centrosymmetric superconductors without strong antiferromagnetic fluctuations. The two mechanisms can act synergistically; for example, spin fluctuations can enhance local magnetic moments, which in turn affect $\langle \mathbf{S} \rangle$ through spin-orbit coupling.

7.1.3 Polaron Effects

Polaron effects arise from strong coupling of charge carriers to optical phonons, resulting in band flattening and mass increase. Their main features include significant optical phonon renormalization and characteristic spectral signatures. The $\mathbf{L} \times \mathbf{E}$ mechanism does not necessarily involve phonons; its spectral features are more associated with electronic and spin excitations. Experimentally, the response of polaron mass enhancement to pressure (via changes in phonon frequency) differs from that of the $\mathbf{L} \times \mathbf{E}$ mechanism (via changes in crystal fields and local electric fields).

7.1.4 Orbital Effects

Pure orbital effects ($\mathbf{L} \cdot \mathbf{S}$ coupling) enhance effective mass by lifting orbital degeneracy. The $\mathbf{L} \times \mathbf{E}$ mechanism represents a distinct coupling channel that requires the simultaneous presence of both orbital angular momentum and local electric fields. In materials with centrosymmetry but strong crystal fields (producing orbital polarization), $\mathbf{L} \cdot \mathbf{S}$ can act alone; whereas in non-centrosymmetric materials, even with quenched orbital angular momentum, the $\mathbf{L} \times \mathbf{E}$ term may still produce finite effects through virtual orbital excitations.

7.2 Unification with Ginzburg-Landau Parameter Constraints

The $\mathbf{L} \times \mathbf{E}$ coupling mechanism provides a microscopic basis for the Ginzburg-Landau parameter constraint $-\alpha \propto m^*$ derived in previous work [4]. The enhancement of m^* through $\mathbf{L} \times \mathbf{E}$ coupling is naturally accompanied by a corresponding enhancement of the pairing strength $-\alpha$ through several mechanisms:

7.2.1 Spin-Orbit Mediated Pairing

In systems with strong spin-orbit coupling, the $\mathbf{L} \times \mathbf{E}$ interaction can enhance pairing through additional scattering channels:

$$-\alpha \propto V_{\text{eff}} \propto V_0 + \lambda_{\text{LE}}^2 \chi_{\text{spin}} \tag{36}$$

where χ_{spin} is the spin susceptibility.

7.2.2 Interface Enhancement

At interfaces, the same inversion symmetry breaking that enhances m^* through $\mathbf{L} \times \mathbf{E}$ coupling can also enhance pairing through modified density of states or additional scattering mechanisms.

7.2.3 Unified Scaling

The joint enhancement of $-\alpha$ and m^* maintains the scaling relation:

$$T_c \propto \sqrt{\frac{-\alpha}{m^*}} \propto \sqrt{\frac{V_{\text{eff}}}{1+\lambda_{\text{LE}}}} \tag{37}$$

This explains how systems with large m^* can still maintain substantial T_c values.

7.3 Theoretical Implications for Superconducting Design

The $\mathbf{L} \times \mathbf{E}$ coupling mechanism suggests new principles for designing superconductors with optimized properties:

7.3.1 Electric Field Optimization

Materials with strong intrinsic electric fields (ferroelectrics, polar materials) may provide optimal platforms for enhancing T_c through the $-\alpha/m^*$ ratio optimization.

7.3.2 Interface Engineering

Artificial heterostructures with controlled inversion symmetry breaking can be designed to optimize the $\mathbf{L} \times \mathbf{E}$ coupling strength for specific applications.

7.3.3 Orbital Moment Enhancement

Materials with large orbital moments (heavy elements, specific crystal field environments) will exhibit stronger $\mathbf{L} \times \mathbf{E}$ coupling and correspondingly larger mass enhancement effects.

7.4 Limitations and Future Directions

While the $\mathbf{L} \times \mathbf{E}$ coupling mechanism provides a promising explanation for Cooper pair inertial mass enhancement, several limitations and future research directions deserve attention:

7.4.1 Quantitative Predictions

The current framework provides qualitative understanding but requires first-principles calculations for quantitative predictions of λ_{LE} values in specific materials.

7.4.2 Strong Correlation Effects

In strongly correlated systems, the simple perturbative treatment of $\mathbf{L} \times \mathbf{E}$ coupling may break down, requiring non-perturbative approaches.

7.4.3 Multiband Systems

The extension to multiband superconductors with complex Fermi surfaces requires more sophisticated treatment of the $\mathbf{L} \times \mathbf{E}$ coupling across multiple bands.

7.4.4 Dynamic Effects

The static treatment of electric fields should be extended to include dynamic field fluctuations and their effect on Cooper pair dynamics.

8 Conclusion

This work has developed a comprehensive theoretical framework identifying $\mathbf{L} \times \mathbf{E}$ coupling as a fundamental mechanism for Cooper pair inertial mass enhancement in superconductors. The core physics, analogous to the increased apparent inertia of a spinning top under a transverse force, involves the coupling of electronic orbital motion to local electric fields, which impedes the establishment of phase coherence without altering the bare electron mass. The key achievements include:

8.1 Theoretical Framework

1. **Mechanism identification**: Established $\mathbf{L} \times \mathbf{E}$ coupling as a distinct mass enhancement pathway operating in non-centrosymmetric systems and systems with strong local electric fields.

2. **Dual enhancement pathways**: Demonstrated that the mechanism operates through both single-particle band renormalization and collective phase fluctuation scattering channels.

3. **Microscopic derivation**: Developed a theoretical foundation connecting the $\mathbf{L} \times \mathbf{E}$ coupling strength to measurable material parameters and fundamental constants.

8.2 Material Applications

The framework successfully explains mass enhancement phenomena across diverse superconducting families:

- **Heavy-fermion systems**: Extreme mass enhancement arises from combination of Kondo physics and enhanced $\mathbf{L} \times \mathbf{E}$ coupling in low-symmetry crystal fields.

- **Iron-based superconductors**: Moderate enhancement with multi-band character reflects the complex Fermi surface and nematic fluctuations in these systems.
- **Interface superconductors**: Giant enhancement effects result from strong built-in electric fields at heterointerfaces.
- **Cuprate superconductors**: Contribution to mass enhancement in systems with charge order or broken inversion symmetry, coexisting with dominant spin fluctuation physics.

8.3 Experimental Verification

The theory generates specific, testable predictions including:

- Electric field tuning of T_c through the m^* modulation
- Characteristic anisotropy in upper critical fields
- Specific signatures in spectroscopic measurements
- Pressure dependence reflecting the coupling strength

8.4 Theoretical Unification

The $\mathbf{L} \times \mathbf{E}$ coupling mechanism provides a microscopic basis for the empirical Ginzburg-Landau parameter constraint $-\alpha \propto m^*$, explaining how systems with enhanced Cooper pair inertial mass can maintain substantial transition temperatures through correlated enhancement of pairing strength.

8.5 Design Principles

The framework suggests new principles for superconducting material design:

- Optimization of intrinsic electric fields through material selection
- Interface engineering for enhanced $\mathbf{L} \times \mathbf{E}$ coupling
- Orbital moment enhancement through heavy element incorporation
- Symmetry control for directional mass enhancement optimization

The $\mathbf{L} \times \mathbf{E}$ coupling mechanism thus represents a fundamental addition to the understanding of Cooper pair inertial mass enhancement, providing new insights for both fundamental understanding and practical design of superconducting materials. Future work should focus on quantitative first-principles calculations, extension to strongly correlated regimes, and experimental verification of the predicted signatures.

Funding

This research received no external funding.

Institutional Review Board Statement

Not applicable.

Informed Consent Statement

Not applicable.

Data Availability Statement

Data sharing is not applicable to this article as no datasets were generated or analyzed during the current study.

Acknowledgments

The author acknowledges the supportive research environment at the Research and Development Center of Huizhou Pustar New Materials Co., Ltd.

Conflicts of Interest

The author declares no conflicts of interest.

References

[1] Ott, H.R.; Rudigier, H.; Fisk, Z.; Smith, J.L. UBe_{13}: An unconventional actinide superconductor. *Phys. Rev. Lett.* **1983**, *50*, 1595-1598.

[2] Tranquada, J.M.; Sternlieb, B.J.; Axe, J.D.; Nakamura, Y.; Uchida, S. Evidence for stripe correlations of spins and holes in copper-oxide superconductors. *Nature* **1995**, *375*, 561-563.

[3] Ge, J.F.; Liu, Z.L.; Liu, C.; et al. Superconductivity above 100 K in single-layer FeSe films on doped $SrTiO_3$. *Nat. Mater.* **2015**, *14*, 285-289.

[4] Yang, D. Physical Processes Underlying Ginzburg-Landau Theory: Energy Competition, Condensation Saturation, and Cooper Pair Inertial Mass Scaling Laws. *Preprint* **2026**.

[5] Ginzburg, V.L.; Landau, L.D. On the theory of superconductivity. *Zh. Eksp. Teor. Fiz.* **1950**, *20*, 1064-1082.

[6] Bardeen, J.; Cooper, L.N.; Schrieffer, J.R. Theory of superconductivity. *Phys. Rev.* **1957**, *108*, 1175-1204.

[7] Gor'kov, L.P. Microscopic derivation of the Ginzburg-Landau equations in the theory of superconductivity. *Sov. Phys. JETP* **1959**, *9*, 1364-1367.

[8] Abrikosov, A.A. On the magnetic properties of superconductors of the second group. *Sov. Phys. JETP* **1957**, *5*, 1174-1182.

[9] Kamihara, Y.; Watanabe, T.; Hirano, M.; Hosono, H. Iron-Based Layered Superconductor La$[O_{1-x}F_x]$FeAs (x = 0.05-0.12) with $T_c = 26$ K. *J. Am. Chem. Soc.* **2008**, *130*, 3296-3297.

[10] Reyren, N.; Thiel, S.; Caviglia, A.D.; et al. Superconducting interfaces between insulating oxides. *Science* **2007**, *317*, 1196-1199.

[11] Stewart, G.R. Heavy-fermion systems. *Rev. Mod. Phys.* **1984**, *56*, 755-787.

[12] Gegenwart, P.; Si, Q.; Steglich, F. Quantum criticality in heavy-fermion metals. *Nat. Phys.* **2008**, *4*, 186-197.

[13] Uemura, Y.J.; et al. Universal correlations between T_c and n_s/m^* in high-T_c cuprate superconductors. *Phys. Rev. Lett.* **1989**, *62*, 2317-2320.

[14] Johnston, D.C. The puzzle of high temperature superconductivity in layered iron pnictides and chalcogenides. *Adv. Phys.* **2010**, *59*, 803-1061.

[15] Homes, C.C.; Dordevic, S.V.; Strongin, M.; et al. A universal scaling relation in high-temperature superconductors. *Nature* **2004**, *430*, 539-541.

[16] Timusk, T.; Statt, B. The pseudogap in high-temperature superconductors: an experimental survey. *Rep. Prog. Phys.* **1999**, *62*, 61-122.

[17] Norman, M.R.; Pines, D.; Kallin, C. The pseudogap: friend or foe of high T_c? *Adv. Phys.* **2005**, *54*, 715-733.

[18] Petrovic, C.; et al. Heavy-fermion superconductivity in $CeCoIn_5$ at 2.3 K. *J. Phys.: Condens. Matter* **2001**, *13*, L337-L342.